Reactivity Descriptors and Rate Constants for Electrophilic Aromatic Substitution: Acid Zeolite Catalyzed Methylation of Benzene and Toluene

Ann M. Vos,[†] Kim H. L. Nulens,[†] Frank De Proft,[‡] Robert A. Schoonheydt,*[,†] and Paul Geerlings[‡]

Center for Surface Chemistry and Catalysis, Katholieke Universiteit Leuven, Kasteelpark Arenberg 23, 3001 Leuven, Belgium and Eenheid Algemene Chemie, Vrije Universiteit Brussel, Pleinlaan 2, 1050 Brussel, Belgium

Received: October 31, 2001

The acid zeolite catalyzed methylation of benzene and toluene with methanol to form toluene and *ortho*-, *meta*-, or *para*-xylene is investigated at the B3LYP/6-31G* level of calculation with a T4 cluster representing the zeolite. After geometry optimization of reactants, transition states and products, reaction rate constants, entropy of activation, activation hardness, and local hardness are calculated and used to model the reactions. In general, the ortho and para products are favored over the meta and nonsubstituted products. Through calculation of rate constants and entropy of activation comparison between different reaction mechanisms has been carried out, indicating that the direct and consecutive mechanisms are competitive at higher temperature. The activation hardness correlates well with the activation energy and local hardness is a good parameter for describing intermolecular reactivity in charge controlled reactions.

1. Introduction

Zeolites, microporous aluminum silicates, have become indispensable as catalysts in the petrochemical industry.[1] One major application is the shape selective production of para-xylene in which a selectivity of 99% can be achieved with a modified MFI-type zeolite.[2] Another application is the industrial important methanol-to-olefine (MTO) process.[3] In both processes, the reaction of methanol with aromatic molecules is a key reaction, as it has been claimed that methylbenzenes are the organic reaction centers in the MTO process.[4] For this reason, the reaction of methanol with benzene and toluene can be seen as a model reaction for zeolite catalyzed reactions and therefor we have chosen this reaction to study theoretically. In general, a reaction catalyzed by a zeolite proceeds via minimum three distinct steps: (1) migration of the reactants to and adsorption on the active site, (2) catalytic reaction and (3) desorption of products. Although an enormous amount of experimental research has been done on electrophilic aromatic substitution (EAS) reactions as catalyzed by acidic zeolites,[1,2−5] the mechanism is still not fully unraveled. Two major questions remain: (1) Does the reaction proceed in one or two steps? and (2) What is the nature of the alkylating agent?

The first question can be rephrased as follows: Can stable intermediates be formed inside the zeolite? From an engineering viewpoint, hydrocarbon conversions are explained by assuming carbenium ions as stable intermediates.[6] But experimentally, only long-lived carbenium ions such as alkyl-substituted cyclopentenyl cation,[7] triphenylmethyl cations[8] and trisubstituted benzenium ions[9] have been observed. Quantum chemical calculations indicate that carbenium ions are transition states rather than reaction intermediates.[10]

The second question relates to the behavior of the alkylation agent (e.g., methanol) inside zeolite pores. Methanol can interact in several distinct ways with zeolites:[11] (1) *end-on adsorption*: the hydroxyl group of methanol is hydrogen bonded with the acid site of the zeolite and the methyl group of methanol points away from the zeolite surface, (2) *side-on adsorption*: the hydroxyl group of methanol is hydrogen bonded with the acid site of the zeolite and the methyl group is in interaction with the zeolite surface, (3) *ion-pair*: the acid proton of the zeolite has jumped to the hydroxyl group of methanol to form CH_3-OH_2^+ and a negatively charged surface site. This interaction is believed to occur at high methanol coverage,[11e−h] (4) *methoxide*: methanol has reacted with the acid site of the zeolite to form water and a methyl group bound to an oxygen of the zeolite lattice, (5) *dimethyl ether (DME)*: two methanol molecules have reacted to form DME that is hydrogen bonded on the acid site of the zeolite.

Experiments on the methylation of benzene or toluene with methanol are usually explained by assuming an Eley−Rideal type mechanism. The methanol strongly adsorbs on the zeolite acid site before it reacts with the aromatic species for which the interactions with the zeolite are much weaker. In the past, a methoxide was assumed to be the reactive species,[12] but more recent in situ studies indicate that methanol and the aromatic coadsorb on the acid site, with methanol in the end-on adsorption mode and the aromatic system in interaction with this methanol molecule.[13]

To gain more insight into the mechanism of zeolite catalyzed reactions quantum chemical calculations can be used.[14] In these calculations, the zeolite is represented by a cluster, e.g., $AlSi_2O_4H_9$. This is a small part cut out of the zeolite lattice and terminated with hydrogens at the dangling bonds to preserve electrostatic neutrality. In this way, the dehydration of methanol to water and a methoxide has been studied by several authors.[11h−i,15] The reaction was found to proceed in one step: the acid proton migrates from an oxygen of the zeolite acid

* To whom correspondence should be addressed. Fax: +32 16 321998. E-mail: robert.schoonheydt@agr.kuleuven.ac.be.
[†] Katholieke Universiteit Leuven.
[‡] Vrije Universiteit Brussel.

10.1021/jp014015a CCC: $22.00
Published on Web 02/01/2002

site to the oxygen of methanol and simultaneously the methyl group moves to another oxygen of the acid site going through only one transition state.

Theoretical investigations on the methylation of benzene or toluene are not so abundant. The hydrogen exchange reaction, the most simple aromatic substitution, is believed to proceed in one step.[16] In this fashion, zeolite catalyzed reactions are similar to gas-phase reactions[17] and not to homogeneous reactions in the liquid phase where a classical two step mechanism with a Wheland intermediate is assumed.[18]

Corma et al.[19] used the HSAB principle to explain the ortho/para selectivity for the methylation of toluene. A combination of the semiempirical AM1 and EEM[20] methods was used by Nulens et al.[21] to investigate the complete reaction path for the methylation of benzene, toluene, and nitrobenzene. Blaszkowski et al.[22] investigated the methylation of benzene and toluene using a density function theory (DFT) method on a $Al(OH)_4H$ cluster. They found that the direct mechanism with coadsorption of methanol and the aromatic molecule is preferred above the consecutive mechanism for which first a methoxide has to be formed before methylation occur. Finally, an attempt was made by Vos et al.[23] to explain the influence of the zeolite lattice on the selectivity for the methylation of toluene by periodic boundary calculations.

In this work, we will investigate the methylation of benzene and toluene with methanol using cluster type DFT-methods. Both the direct and the consecutive mechanism are investigated. Cluster type methods have the advantage over periodic boundary methods that they can be used to gain deeper insight in the reactions by calculation of reaction rate constants and by evaluation of density functional based reactivity descriptors such as the hardness and Fukui functions of the systems. Both strategies are used in this work, enabling us to use properties of both the transition states (via reaction rates) and the reactants (DFT-based reactivity descriptors) to get an idea why things are happening the way they do. The reactivity descriptors are evaluated at ab initio level as will be explained in the method part.

2. Theoretical Background and Method

2a. Geometry Optimization. All reactants, transition states, intermediates, and products that are observed in the reaction are localized with cluster type calculations. During the geometry optimization, we look for a local minimum for reactants, adsorbed complexes, and products and for a first order saddle point for transition states. On the stationary points frequencies are evaluated analytically to check whether the obtained structures have the correct number of imaginary frequencies: none for minima and one for transition states.

The cluster we used, consists of four T-atoms (one Al and three Si) and was allowed to relax completely during the optimizations. The DFT calculations used the B3LYP functional[24] and a 6-31G* basisset. They were done with *Gaussian98*.[25]

2b. Reaction Rate Constants. The reaction rate constants of all studied reactions are evaluated by using the canonical transition state theory of Eyring, Evans, and Polanyi.[26] The general expression for the reaction rate constant k_r is

$$k_r = \frac{k_B T}{h} \cdot \frac{Q^{\ddagger}}{\prod_i Q_i} \cdot e^{-E_{bar}/RT} \qquad (1)$$

with k_B and h the constants of Boltzman and Planck constants, and T is the temperature. E_{bar} is the activation barrier of the reaction. It is the energy difference between the reactants and the transition state containing already the zero point energy corrections. Q_i and $Q^{\ddagger}$ represent the partition function of reactants and transition state (the index i running over all reactants). The exponential dependence on the energy barrier is the natural consequence of the assumption that the system has a Maxwell−Boltzman energy distribution. The reaction coordinate is not included in the evaluation of $Q^{\ddagger}$, but is considered as a separate translation mode. It's partition function, combined with the expression for the average velocity by which the transition state is crossed, is responsible for the appearance of the factor k_BT/h. For the evaluation of eq 1, we used a rigid rotor harmonic oscillator approximation[24] and we assumed that rotational (r), vibrational (υ) and electronic (e) movements are independent of each other to get

$$Q = Q_t \cdot Q_r \cdot Q_v \cdot Q_e \qquad (2)$$

where Q_t is the translational partition function.

Applied to the reaction of a given molecule A with a zeolite, HZ, the reaction rate constant per acid proton becomes

$$k_r = (N_A V)\left(\frac{k_B T}{h}\right) \cdot \frac{(Q_v^{\ddagger} Q_r Q_t)_{TS}}{(Q_v Q_r Q_t)_A (Q_v Q_r Q_t)_{HZ}} \cdot e^{-E_{bar}/RT} \qquad (3)$$

N_A, Avogadro's number and V, the volume of one mol A, appear because of the use of concentration in the rate laws. For two molecules A and B reacting simultaneously with a zeolite, the reaction rate per acid proton becomes

$$k_r = (N_A V)^2 \times \left(\frac{k_B T}{h}\right) \cdot \frac{(Q_v^{\ddagger} Q_r Q_t)_{TS}}{(Q_v Q_r Q_t)_A (Q_v Q_r Q_t)_B (Q_v Q_r Q_t)_{HZ}} \cdot e^{-E_{bar}/RT} \qquad (4)$$

When A and B react in a consecutive mechanism with the zeolite the expression becomes

$$k_r = (N_A V) \times \left(\frac{k_B T}{h}\right) \cdot \frac{(Q_v^{\ddagger} Q_r Q_t)_{TS2} (Q_v Q_r Q_t)_C}{(Q_v Q_r Q_t)_A (Q_v Q_r Q_t)_B (Q_v Q_r Q_t)_{HZ}} \cdot e^{-E_b + E_a - E'_a/RT} \qquad (5)$$

with *TS2* being the transition state of the second step and *C* the product formed in the first step that does not react any further in the second step. E_a is the activation barrier for the first step, E'_a for the first step in reverse and E_b for the second step. The derivation of eq 5, which can be found in the Appendix, assumes a two step reaction under steady-state conditions.

The molecular partition functions are obtained after a vibrational analysis by *Gaussian98*, where the frequencies were scaled according to the procedure proposed by Scott et al.[27] With eqs 4 and 5, we calculated the rate constants for a temperature ranging from 300 to 800 K.

Kinetic data are often analyzed in terms of an Arrhenius expression[26b]

$$k_r = A e^{-E_{arr}/RT}$$

$$\ln k_r = \ln A - \frac{E_{Arr}}{RT} \qquad (6)$$

where E_{Arr} is the Arrhenius activation energy and A the preexponential factor. When $\ln(k_r)$ is plotted against T^{-1}, a

straight line is obtained with slope $-E_{\mathrm{Arr}}\,R^{-1}$ and intercept ln(*A*). The preexponential factor, *A*, is proportional to the entropy difference between reactants and transition state, ΔS_{act}[26c]

$$\Delta S_{\mathrm{act}} = R\left[\ln A - \ln\left(\frac{k_{\mathrm{B}}T}{h}\right) - (1-\Delta n) + \ln V^{\Delta n}\right] \quad (7)$$

where Δn is the change in the number of molecules from the reactants to the transition state.

2c. Density Functional Based Reactivity Descriptors. Density functional theory[28] (DFT) provides a framework to discuss reactions in terms of changing number of electrons (N) and/or changing external potential $v(\mathbf{r})$ (i.e., due to the nuclei). Within this conceptual branch of DFT the global hardness, η, is defined as the second derivative of the energy, E, with respect to the number of electrons, N [29]

$$\eta = \frac{1}{2}\left(\frac{\partial^2 E}{\partial N^2}\right)_{v(\mathrm{r})} = \frac{1}{2S} \quad (8)$$

where S is the global softness. In the finite difference approach η can be written as

$$\eta = \frac{IE - EA}{2} \quad (9)$$

with IE and EA the first vertical ionization energy and the electronaffinity of the molecule. In the frozen core approximation, η equals the HOMO−LUMO gap

$$\eta = \frac{E_{\mathrm{LUMO}} - E_{\mathrm{HOMO}}}{2} \quad (10)$$

The Fukui function $f(\mathbf{r})$, as defined by Parr and Yang,[30] is a mixed second derivative of the energy of the system with respect to N and the potential $v(\mathbf{r})$

$$f(\mathbf{r}) = \left(\frac{\partial^2 E}{\partial N \partial v(\mathbf{r})}\right) = \left[\frac{\delta \mu}{\delta v(\mathbf{r})}\right]_N = \left(\frac{\partial \rho(\mathbf{r})}{\partial N}\right)_{v(\mathbf{r})} \quad (11)$$

where μ represents the electronic chemical potential and $\rho(\mathbf{r})$ the electron density. The Fukui function describes the sensitivity of the chemical potential of a system to an external potential perturbation. It is a reactivity index for orbital controlled reactions: the larger the value of the Fukui function, the higher the reactivity.[31]

Because of the discontinuity of the derivative of the electron density with respect to the number of electrons, Parr and Yang[30] associated a left ($f^-(\mathbf{r})$) and right ($f^+(\mathbf{r})$) side derivative with the Fukui function, corresponding to an electrophilic and nucleophilic attack, respectively. Using a finite difference approximation, both functions can be written as

$$f^+(\mathbf{r}) = \rho_{\mathrm{N+1}}(\mathbf{r}) - \rho_{\mathrm{N}}(\mathbf{r}) \quad (12)$$

$$f^-(\mathbf{r}) = \rho_{\mathrm{N}}(\mathbf{r}) - \rho_{\mathrm{N-1}}(\mathbf{r}) \quad (13)$$

where $\rho_{\mathrm{N}}(\mathbf{r})$, $\rho_{\mathrm{N+1}}(\mathbf{r})$, and $\rho_{\mathrm{N-1}}(\mathbf{r})$ are the electron densities of the N, N+1 and N−1 electron system, all calculated at the same external potential $v(\mathbf{r})$ of the N electron system.

Yang and Mortier[32] introduced the condensed form of the Fukui function, i.e., the Fukui function per atom k in a molecule using atomic populations

$$f_k^+ = [q_k(N+1) - q_k(N)] \quad (14)$$

$$f_k^- = [q_k(N) - q_k(N-1)] \quad (15)$$

with q_k the populations of atom k in the molecule. The atomic charges can be obtained by a ChelpG population analysis[33] using a B3LYP/6-31G* level of calculation in *Gaussian98*.

Because the local softness, $s(\mathbf{r})$, is related to the Fukui function through $s(\mathbf{r}) = S \cdot f(\mathbf{r})$, the condensed local softness is related to the condensed Fukui function via[34]

$$s_k^i = f_k^i \cdot S \quad i = + \text{ or } - \quad (16)$$

Both f_k and s_k describe local properties of the molecules thus allowing the possibility to discriminate between the reactivity of distinct atoms in a molecule. s_k is used in the local HSAB principle[35] which states that the original HSAB principle of Pearson[36] is still valid at the atomic level: soft atoms react preferentially with other soft atoms. To complete the analogy between local and global HSAB principle the local hardness[37] is required.

Although the definition of a counterpart of the local softness $s(\mathbf{r})$, the local hardness $\eta(\mathbf{r})$, turned out to be not unambiguous,[38] it is clear from previous work by Berkowitz et al.[37] and some of the present authors[39] that local hardness bears some analogy with the molecular electrostatic potential. The local hardness has been put in relation with the electrostatic potential[37−39] and since ChelpG charges are derived from the same electrostatic potential[33] we used these charges as an approximation for the condensed local hardness

$$\eta_k \cong q_k \quad (17)$$

The atomic charge can be used as a measure for the local hardness as they both quantify essentially the local reactivity in charge controlled reactions or reaction steps.[39] Obviously, the actual values q_k are dependent on the method used, trends however can be expected to remain unaltered with the basis set used in the present work.

3. Results and Discussion

By calculating the geometry and energy of all species involved in the reaction, we found all the possible steps of the reaction mechanism. This was the starting point of our analysis and these results will be described first (section 3a). For the methylation of benzene, we investigated both the consecutive reaction mechanism and the direct mechanism. For the methylation of toluene, only the direct reaction mechanism was investigated. Subsequently, reaction rate constants of all the reactions are calculated for comparison with experimental data (section 3b). Finally, to get better insight in the reaction and to know the driving force behind it, we calculated reactivity descriptors that are given in the last sections (section 3c−d).

3a. Reaction Paths for Methylation of Benzene and Toluene. The first reaction that was studied, methylation of benzene in a consecutive mechanism, proceeds in two consecutive steps (step 1a and 1b) as can be seen in Figure 1. In Figure 2 all the optimized geometries are shown, with their label: **R** for adsorbed reactants, **TS** for transition states and **P** for adsorbed products, **1a** for structures involved in the first step and **1b** for structures involved in the second step. First, methanol adsorbs on the Brønsted acid site (**R1a**, see Figure 2). During the reaction, the acid proton of the cluster jumps to the hydroxyl of methanol and in the transition state (**TS1a**, see Figure 2) the planar methyl is halfway between the methanol oxygen and the bridging oxygen where it will be attached to after reaction.

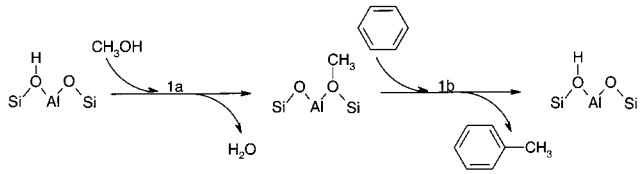

Figure 1. Reaction scheme of the two step consecutive mechanism for the methylation of benzene with methanol.

TABLE 1: Geometrical and Energetical Characteristics for the First Step of the Consecutive Mechanism (formation of methoxide)[a]

	R1a	TS1a	P2a
AlO_1	1.899	1.778	1.728
AlO_2	1.717	1.804	1.893
AlO_1Si_1	120.1	138.0	142.6
AlO_2Si_2	176.7	136.3	111.7
O_1H_a	1.024	3.317	2.164
H_aO_m	1.564	0.979	0.973
O_mC_m	1.431	1.765	3.201
C_mO_2	5.139	2.257	1.462
dihedral methyl	35.76	15.36	33.35
$O_1H_aO_m$	159.2	112.2	133.7
$O_mC_mO_2$	56.4	165.6	90.6
ΔE_{act}		220.80	
imaginary frequency of TS		−270.48	

[a] Distances are in Å, angles in degrees, energies in kJ mol^{-1} and the imaginary frequency at the transition state in cm^{-1}.

(**P1a**). The energy barrier between the **R1a** and the **TS1** is 220.8 kJ mol^{-1} (including ZPE) and the reaction energy is 43.4 kJ mol^{-1}. The geometry can be seen in Table 1. In the second reaction step benzene adsorbs on the methoxy cluster (**R1B**). After the migration of the methyl to benzene and the back-donation of a proton to the cluster via a second transition state (**TS1b**) the final products are formed (**P1b**). (see Figure 2) The activation energy (including ZPE) of this step is 186.4 kJ mol^{-1}. The geometry can be seen in Table 2.

TABLE 2: Geometrical and Energetical Characteristics for the Second Step of the Consecutive Mechanism (methylation of benzene)[a]

	R1b	TS1b	P2b
AlO_1	1.708	1.774	1.932
AlO_2	1.892	1.801	1.730
C_mO_2	1.450	2.348	3.860
C_bC_m	4.036	1.943	1.511
C_bH_b	1.086	1.090	2.465
H_bO_1	3.668	3.853	0.985
$O_mC_mO_2$	109.4	169.7	86.2
$O_1H_bC_b$	102.0	114.4	151.1
dihedral methyl	34.32	−19.54	−37.70
ΔE_{act}		186.4	
imaginary fequency of TS		−325.02	

[a] Distances are in Å, angles in degrees, energies in kJ mol^{-1} and the imaginary frequency at the transition state in cm^{-1}.

The direct mechanism for the methylation of benzene proceeds in one step as can be seen in Figures 3 and 4. Methanol and benzene coadsorb on the acid site (**R2**). Methanol is adsorbed by two hydrogen bonds on the cluster. The methyl group of methanol is in interaction with benzene. During reaction the proton of the acid site, H_a migrates to the oxygen of methanol to form water and the methyl group of methanol will move to benzene (**TS2**). Finally benzene gives back a proton, H_{ar} to the zeolite cluster (**P2**). The geometrical and energetical parameters of the different species involved in the reaction can be seen in Table 3. At the transition state the acid proton, H_a, is already attached to the oxygen of methanol, O_m. The methyl group is halfway between O_m and C_{ar} and the proton of benzene, H_{ar} has not moved yet.

None of the previous described reaction steps is concerted. Donation of a proton (or methyl group in case of reaction 1b)

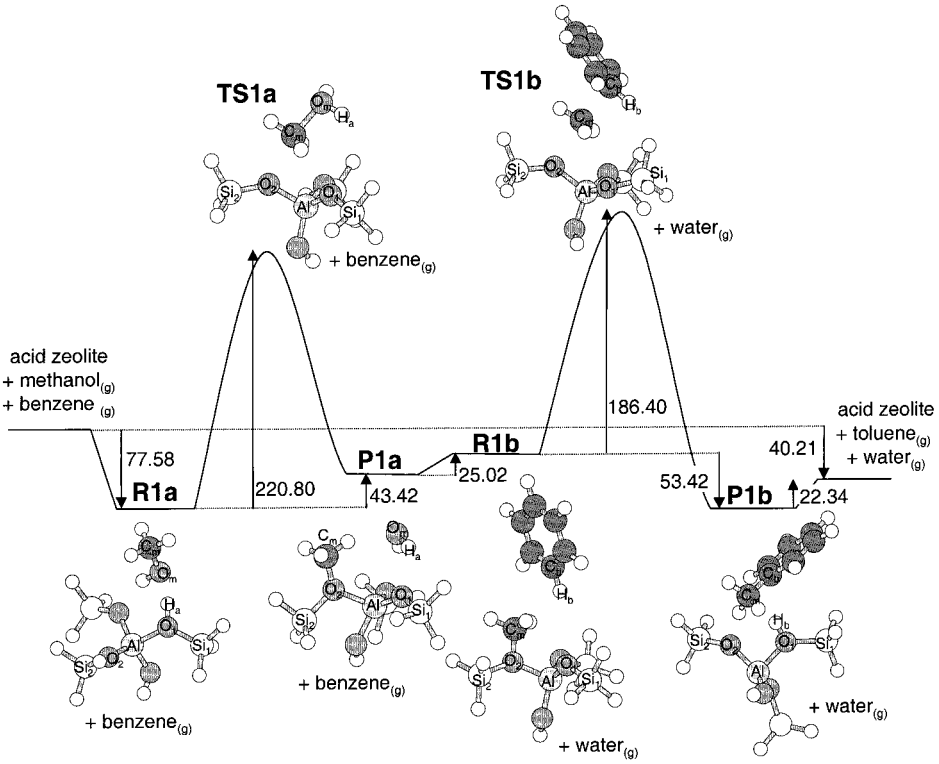

Figure 2. Reaction diagram for the two step consecutive mechanism for the methylation of benzene with methanol with geometries and energy differences (including ZPE, in kJ mol^{-1}). **R1a**, **TS1a**, and **P1a** are respectively the reactants the transition state and the products of the first step (formation of methoxide). **R1b**, **TS1b**, and **P1b** are the reactants the transition state and the products of the second step (methylation of benzene).

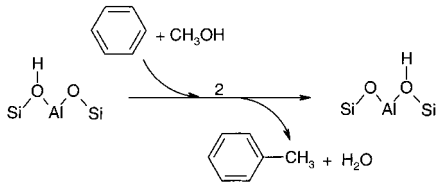

Figure 3. Reaction scheme of the one step direct mechanism for the methylation of benzene with methanol.

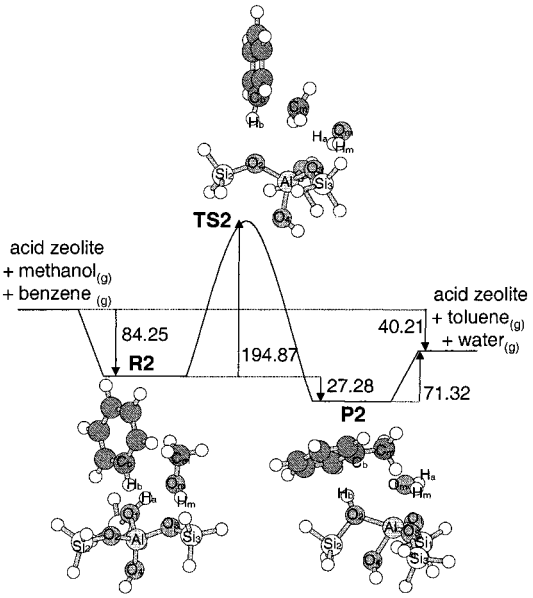

Figure 4. Reaction diagram for the one step direct mechanism for the methylation of benzene with methanol with geometries and energy differences (including ZPE, in kJ mol^{-1}). **R2**, **TS2**, and **P2** are respectively the reactants, the transition state and the products of the reaction.

from zeolite cluster to molecule(s) occurs always earlier in the reaction than back-donation of a proton (or methyl group in case of reaction 1a) to the zeolite cluster. These asynchronous reaction paths, however, never result in the formation of stable charged intermediates.

Because it is believed that the direct mechanism is the preferred one for methylation of aromatics,[13a] we only investigated this route for the methylation of toluene in the formation of *ortho*-, *meta*-, and *para*-xylene. These reactions proceed very much along the same paths as described for the methylation of benzene. The starting point of the reaction is the coadsorption of toluene and methanol on the acid site. This starting point is slightly different for each reaction leading to one of the three xylenes. The adsorbed reactants leading to *ortho*-xylene are named **oR**, to *meta*-xylene **mR** and to *para*-xylene **pR**. Accordingly, the three different transition states and the three different products are named: **oTS**, **mTS**, **pTS**, **oP**, **mP**, and **pP**. In Table 3, the geometry- and energy-differences for the three reactions are given. The adsorption energies are almost identical. The values of ΔE_{bar} follow the same order as for homogeneous reactions: the methyl substituent of toluene is an activating ortho-/para-directing group.

The one step, asynchronous pathway is in agreement with previous studies, wherein no stable charged intermediate for acid zeolite catalyzed reactions was found.[10,11,14−16,19,21−23] Even when the Coulombic interactions, van der Waals interactions or steric constraints of the zeolite lattice are included, the mechanism remains unchanged.[23] Inclusion of these effects however results in lower activation energies, possibly due to the extra stabilization of the charged transition states. Though, comparison of the activation energies obtained from cluster calculations and crystal calculations is not straightforward. They have been obtained with different basis sets and exchange-correlation functionals, which have an effect on energies and atomic distances.

3b. Reaction Rate Constants. In the temperature range of 300 to 800 K we have calculated the reaction rate constants for the above-described reactions as explained in section 2b. The results can be seen in Table 4, where the rate constants are given for 400 K together with the kinetic parameters resulting form the Arrhenius plot (Figure 5). The temperature of 400 K was chosen to allow better comparison with experimental results.[13a]

At low temperature the direct mechanism is the fastest one and the consecutive mechanism becomes competitive with the direct mechanism at higher temperature. The rate for formation of the different xylene isomers follows for all temperatures the order: para > ortho > meta, the meta value being close to benzene, in agreement with the electron donating ortho-, para-directing influence of the methyl group.

In Figure 5 Arrhenius plots are given. The Arrhenius activation energy (see Table 4) for the consecutive mechanism is much higher than for the direct mechanism, but also the

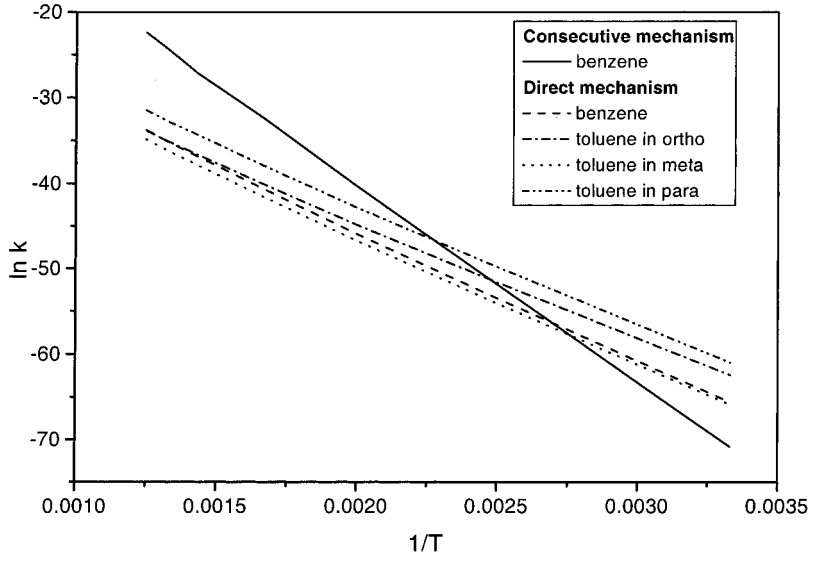

Figure 5. Reaction rate constants at temperature interval 300−800 K. Arrhenius plot with $\ln(k_r)$ in functions of T^{-1}.

TABLE 3: Geometrical and Energetical Characteristics for the Direct Mechanism: Methylation of Benzene and Toluene in *para*, *meta*, and *ortho*[a]

	R2	TS2	P2	*o*R	*o*TS	*o*P	*m*R	*m*TS	*m*P	*p*R	*p*TS	*p*P
OH_a	1.030	1.896	2.143	1.031	1.852	2.131	1.030	1.896	2.139	1.030	1.899	2.154
$AlOH_a$	110.7	107.1	130.4[b]	110.8	106.6	131.3[b]	110.8	106.8	130.4[b]	110.7	106.7	130.3[b]
AlC_m	4.480	3.457	4.615	4.487	3.514	5.253	4.488	3.462	4.457	4.499	3.467	4.562
H_aO_m	1.541	0.984	0.977	1.541	0.987	0.977	1.544	0.984	0.977	1.544	0.985	0.977
H_mO_3	1.842	1.909	2.128	1.848	1.922	2.139	1.842	1.902	2.141	1.843	1.874	2.145
O_mC_m	1.435	2.328	3.832	1.435	2.278	3.703	1.435	2.320	3.612	1.435	2.281	3.586
C_mC_{ar}	3.938	1.963	1.511	3.925	1.998	1.510	3.923	1.971	1.512	3.917	1.998	1.511
$C_{ar}H_{ar}$	1.086	1.096	2.873	1.087	1.091	2.775	1.086	1.095	2.697	1.086	1.093	2.882
$H_{ar}O_2$	2.829	2.107	0.976	2.756	2.321	0.976	2.797	2.140	0.997	2.802	2.180	0.976
$O_mC_mC_{ar}$	95.6	169.8	83.1	95.2	171.3	73.2	95.9	170.5	89.0	90.5	171.0	85.0
dihedral CH_3	35.32	−17.18	−37.86	35.49	−14.86	−38.27	35.53	−16.20	−37.88	35.78	−14.57	−38.02
ΔE_{act}		194.84			182.34			191.74			185.43	
imaginary frequency of TS		−339.63			−372.95			−344.76			−372.59	

[a] Distances are in Å, angles in degrees, energies in kJ mol^{-1} and the imaginary frequency at the transition state in cm^{-1}. [b] $AlOH_{ar}$-angle.

TABLE 4: Reaction Rate Constants (k_r) at 400 K in m^6 mol^{-2} s^{-1} Calculated by the Transition State Theory, Activation Energy (E_{Arr}) in kJ mol^{-1}, Pre-exponential Factors (A) in m^6 mol^{-2} s^{-1}, Entropy of Activation (ΔS_{act}) in kJ K^{-1} mol^{-1} Calculated Using the Arrhenius Theory

	k_r at 400K	E_{Arr}	A	ΔS_{act}
consecutive	2.834×10^{-23}	192.81	5.166×10^{2}	−0.115
step 1	7.754×10^{-17}	153.87	1.137×10^{4}	−0.086
step 2	9.708×10^{-22}	190.51	8.624×10^{3}	−0.091
direct				
benzene	5.604×10^{-24}	127.12	3.025×10^{-7}	−0.300
toluene	3.621×10^{-23}	114.15	3.950×10^{-8}	−0.317
ortho				
meta	3.067×10^{-24}	123.93	6.333×10^{-8}	−0.313
para	2.226×10^{-22}	117.78	7.242×10^{-7}	−0.293

preexponential factor is higher. This is the reason at higher temperature the consecutive mechanism can compete with the direct mechanism. With eq 7, ΔS_{act} can be calculated and because the values are practically constant over the temperature interval, only the values at 400 K are given (see Table 4). The negative ΔS_{act} values indicate a decrease in entropy when going from reactants to transition state due to the loss of rotational and translational degrees of freedom. ΔS_{act} for the consecutive mechanism is less negative than for the direct mechanism: The consecutive mechanism is entropically favored because only one molecule at a time interacts with the active site, whereas for the direct mechanism two molecules at a time must interact with the active site.

In addition, the values for the free energy of activation, $\Delta G_{act} = \Delta H_{act} - T\Delta S_{act} = E_{Arr} - 2RT - T\Delta S_{act}$, for the two reaction mechanisms are close together: at 400 K ΔG_{act} is 232 kJ mol^{-1} and 240 kJ mol^{-1} for respectively the consecutive and direct mechanism for methylation of benzene. Or the activation entropy compensates for the activation energy in the expression for the rate constant.

The preference for the direct mechanism at lower temperatures is in agreement with the literature where in situ ^{13}C MAS NMR measurements indicate that methoxides are less reactive and only coadsorbed methanol is responsible for the methylation of toluene.[13a]

The validity of the obtained rate constants was tested via additional calculations for the H/D-exchange reaction of methane catalyzed by acid zeolites.[40] The transition state of this reaction was already optimized[41] and reliable experimental results are available.[42] The calculated reaction rate constants seemed to give a lower limit for high alumina zeolites.

3c. Density Functional Based Global Reactivity Descriptors. Table 5 shows the values for the hardness, η, of the adsorbed reactants (**R1a**, **R1b**, **R2**, **oR**, **mR**, **pR**), the transition states (**TS1a**, **TS1b**, **TS2**, **oTS**, **mTS**, **pTS**) and the adsorbed products (**P1a**, **P1b**, **P2**, **oP**, **mP**, **pP**), together with the activation hardness, $\Delta\eta_{act} = \eta_{TS} - \eta_{reactants}$. η is calculated using two different procedures: (1) from the HOMO−LUMO gap using eq 10, and (2) using the finite difference approach according eq 9.

TABLE 5: Hardness, η, of the Adsorbed Reactants (R1a, R1b, R2, oR, mR, pR), the Transition States (TS1a, TS1b, TS2, oTS, mTS, pTS) and the Adsorbed Products (P1a, P1b, P2, oP, mP, pP), Together with the Activation Hardness, $\Delta\eta_{act} = \eta_{TS} - \eta_{reactants}$, Both in Atomic Units[a]

	HOMO−LUMO gap				(IE-EA)/2			
	$\eta_{reactants}$	η_{TS}	$\eta_{products}$	$\Delta\eta_{act}$	$\eta_{reactants}$	η_{TS}	$\eta_{products}$	$\Delta\eta_{act}$
consecutive								
step 1	0.1334	0.0921	0.1346	0.0413	0.1935	0.1637	0.1955	0.0298
step 2	0.1233	0.0485	0.1166	0.0748	0.1823	0.1143	0.1747	0.0680
direct								
benzene	0.1192	0.0595	0.0057	0.0597	0.1781	0.1250	0.1755	0.0534
toluene								
ortho	0.1141	0.0648	0.1174	0.0493	0.1730	0.1287	0.1750	0.0443
meta	0.1144	0.0607	0.1151	0.0536	0.1957	0.1250	0.1725	0.0707
para	0.1132	0.0633	0.1248	0.0499	0.1722	0.1270	0.1727	0.0452

[a] η is calculated using two different procedures: (1) from the HOMO−LUMO gap using eq 10, and (2) using the finite difference approach according eq 9.

The adsorbed reactants and products are much harder than the transition states ($\eta_{reactants}$, $\eta_{products} > \eta_{TS}$). According to the original definition of the terms "hard" and "soft",[36] hard compounds have a lower polarizability than soft compounds. Because transition states possess more delocalized electrons they are more polarizable than reactants and products. The fact that reactants and products are much harder than transition states can also be explained by the maximum hardness principle:[43] molecules arrange themselves so as to be as hard as possible. Therefore, stable structures with low energy (here reactants and products) are likely to be harder than less stable structures with high energy (here transition states).

According to Zhou et al.[44] the activation hardness, $\Delta\eta_{act} = \eta_{TS} - \eta_{reactants}$, is proportional to the activation energy and can be used to predict the selectivity of EAS reactions. With η being approximated as the HOMO−LUMO gap, we get for $\Delta\eta_{act}$ the order: ortho < para < meta < benzene. This is the same order as we obtained for the activation energies (see Tables 5 and 3).

When calculated with the finite difference approach (equation 9), $\Delta\eta_{act}$ gives the order ortho < para < benzene < meta. The high $\Delta\eta_{act}$ for meta is caused by the fact that the hardness of **mR** differs strongly from the others. In general, non finite

TABLE 6: ChelpG Charges in Atomic Units of the Atoms Involved in the Reaction for the Adsorbed Reactants (R1a, R1b, R2, oR, mR, pR), the Transition States (TS1a, TS1b, TS2, oTS, mTS, pTS) and the Adsorbed Products (P1a, P1b, P2, oP, mP, pP)

	q_{Ca}	q_{Cm}	q_{Ha}	q_{Om}	q_{O1}	q_{O2}	q_{Har}
reactants							
consecutive							
step 1		0.1510	0.4609	−0.6197	−0.6357	−0.6866	
step 2	−0.0672	−0.1040			−0.6315	−0.2690	0.0829
direct							
benzene	−0.0259	0.1489	0.4021	−0.5978	−0.5440	−0.5966	0.0634
toluene							
ortho	−0.1522	0.1744	0.4166	−0.6093	−0.5568	−0.6049	0.087
meta	−0.0033	0.1621	0.4202	−0.6109	−0.5545	−0.6019	0.0649
para	−0.0548	0.1443	0.4495	−0.6068	−0.6103	−0.6357	0.0712
TS							
consecutive							
step 1		−0.0790	0.4498	−0.5651	−0.7793	−0.6644	
step 2	0.1914	0.0714			−0.7478	−0.6352	0.0251
direct							
benzene	0.2143	−0.0514	0.3862	−0.7149	−0.6887	−0.6020	−0.0315
toluene							
ortho	0.0438	−0.0427	0.4060	−0.7177	−0.7305	−0.5920	0.0305
meta	0.2239	−0.0525	0.3922	−0.7171	−0.7082	−0.6191	−0.0088
para	0.1514	−0.0438	0.3942	−0.7156	−0.7062	−0.6169	−0.0006
products							
consecutive							
step 1		−0.1653	0.3993	−0.7595	−0.2713	−0.7271	
step 2	0.2642	−0.3096			−0.6676	−0.6603	0.3926
direct							
benzene	0.1800	−0.2660	0.3883	−0.6899	−0.6999	−0.5768	0.3829
toluene							
ortho	0.1110	−0.1780	0.3931	−0.6900	−0.7023	−0.5303	0.3514
meta	0.2206	−0.2883	0.3798	−0.6801	−0.6924	−0.5602	0.3691
para	0.1596	−0.2655	0.3817	−0.6794	−0.7096	−0.5597	0.3643

TABLE 7: Local Reactivity Indices (in atomic units) for the Adsorbed Reactants of the Direct Mechanisms (R2, oR, mR, pR)[a]

	Δs_{CC}	η_{Car}	$\Delta\eta_{CC}$	$\Delta E_{CC}/10^{-4}$	$\Pi\eta_{CC}$
benzene	0.0777	0.0259	0.1230	−9.847	0.0039
toluene					
ortho	0.0105	0.1522	0.0222	−67.629	0.0265
meta	0.2197	0.0033	0.1588	−1.363	0.0005
para	0.5128	0.0548	0.0895	−20.190	0.0079

[a] For definition of Δs_{CC}, $\Delta\eta_{CC}$, ΔE_{CC}, and $\Pi\eta_{CC}$, see text.

difference methods may shed some light on this sequence, but they are too demanding to be applied on the present case.[45]

Although in general the hardness profile for a reaction rarely shows its minimum exactly at the transition state, trends in activation hardness values (by definition taken at the transition state) might be considered to be in line with those of the hardness minima,[46] accounting for the maximum hardness principle.

3d. Local Reactivity Descriptors and the Local HSAB Principle. Table 6 shows the charges of the atoms involved in the reaction, calculated for adsorbed reactants (**R1a**, **R1b**, **R2**, **oR**, **mR**, **pR**). These atomic charges were used in the evaluation of the local reactivity indices of Table 7.

According to the local HSAB principle, soft atoms react preferentially with other soft atoms and hard atoms with other hard atoms. For orbital controlled reactions where the soft−soft interactions dominate, Δs between reacting atoms must be as small as possible (softness matching) and analogously, for charge controlled reactions where the hard−hard interactions dominate, $\Delta\eta$ between reacting atoms must be as small as possible.

We here fore evaluated $\Delta s_{CC} = s^+_{Cm} - s^-_{Car}$, the differences in local softness between C of the attacking methyl group and C of benzene or toluene that undergoes the electrophilic attack, two atoms that will be bonded after reaction (Table 7). For the evaluation of s^+_{Cm} and s^-_{Car} eqs 14−16 were used. Δs_{CC} follows the order: ortho < benzene < meta < para, in disagreement with experiment.

$\Delta\eta_{CC}$, the difference in local hardness between C of the attacking methyl group and C of benzene or toluene that undergoes the electrophilic attack is approximated by the difference in ChelpG atomic charges: $|q_{Cm}| - |q_{Car}|$ (see Table 7). Here, we obtain the order ortho < para < meta, in agreement with experiment. For benzene, $\Delta\eta_{CC}$ is smaller than for meta.

According to the differences in local condensed softnesses, Δs_{CC}, ortho is favored over benzene and then meta and para, whereas according to the differences in local condensed hardnesses, $\Delta\eta_{CC}$, ortho is favored over para and then benzene and meta. The local softness does not turn out to be a good reactivity descriptor for this reaction in contrast to the local hardness. Because the actual electrophilic species, CH_3^+, is a hard reactant, the reaction is not dominated by soft−soft interaction but by hard−hard interactions or the reaction is charge controlled.

For charge controlled reactions the electrostatic interactions are dominant. The strength of these interactions is proportional to the electrostatic interaction energy

$$\Delta E_{CC} \propto \frac{q_{Car} q_{Cm}}{R_{CC}} \tag{18}$$

R_{CC} being the distance between C_{ar} and C_m. Values are given in Table 7 and indicate that the interaction is strongest for *ortho*, followed by *para* and *meta*. The value for benzene lies between *para* and *meta*. Since $\eta_k \cong q_k$, the product of the atomic hardnesses, $\Pi\eta_{CC}$, can also measure the interaction strength. Again the order ortho > para > benzene > meta is obtained (Table 7).

So far three different indices, for describing hard−hard interactions ($\Delta\eta_{CC}$, ΔE_{CC}, and $\Pi\eta_{CC}$), give the reactivity sequence ortho > para > benzene > meta.

4. Conclusion

In this study, we went into a detailed description of rate and mechanism of the different elementary reaction steps for the methylation of benzene and toluene catalyzed by acidic zeolites. The reactions proceed in an asynchronous pathway as supported by the transition state geometries. Like in other studies of acid zeolite catalyzed reactions, no stable charged intermediates are formed during reaction. Clusters are only local models for zeolite catalyzed reactions and do not include possible stabilization or steric constraints imposed by the zeolite lattice. When these effects are included by periodic boundary calculations, the mechanism remains unchanged (one step, asynchronous pathway) but the activation energies are lower due to the electrostatic stabilization of the zeolite framework.[23]

Cluster models have the advantage that they can be used for the evaluation of reaction rate constants, entropy of activation, activation hardness and local hardness. These characteristics

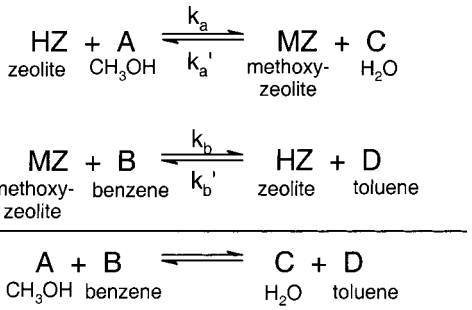

Figure 6. Reaction scheme.

were used here to model the reactions. In general the ortho and para products are favored over the meta and nonsubstituted products.

Comparison between different reaction mechanisms can be carried out through calculation of reaction rate constants. The consecutive mechanism has a higher Arrhenius activation energy but is entropically favored over the direct mechanism. Therefore both mechanisms are competitive at higher temperature.

The activation hardness correlates well with the activation energy. DFT-based local reactivity descriptors indicate that as in the original HSAB principle of Pearson there is a hard-like-hard and soft-like-soft rule operating at local level, local hardness, and local softness not being simple reciprocals of each other. Local hardness turns out to be a good parameter for describing intermolecular reactivity in charge controlled reactions.

Acknowledgment. This work has been performed with support from the G.O.A. (Geconcerteerde Onderzoeksactie Vlaanderen). The authors acknowledge the Free University of Brussels (V.U.B.) for a generous computer grant. A.M.V. thanks the I.W.T for financial support and P.G. thanks the Fund for Scientific Research-Flanders (F.W.O) for continuous support of his group.

Appendix

The formula for calculating the global reaction rate constant of the consecutive mechanism can easily be derived starting from the two steps reaction scheme,[47] depicted in Figure 6. For easy writing of the formulas *HZ* stands for the catalyst (acid zeolite), *MZ* for the intermediate (methoxy-zeolite) and *A*, *B*, *C*, and *D* for methanol, benzene, water, and toluene, respectively.

1st Assumption: second reaction is a nonequilibrium reaction

$$\frac{\mathrm{d[D]}}{\mathrm{d}t} = k_b[\mathrm{MZ}][\mathrm{B}] \tag{A.1}$$

[*MZ*] is not known but under steady-state conditions

$$\frac{\mathrm{d[D]}}{\mathrm{d}t} = 0 = k_a[\mathrm{HZ}][\mathrm{A}] - k_a'[\mathrm{MZ}][\mathrm{C}] - k_b[\mathrm{MZ}][\mathrm{B}] \tag{A.2}$$

$$[\mathrm{MZ}] = \frac{k_a[\mathrm{HZ}][\mathrm{A}]}{k_a'[\mathrm{C}] + k_b[\mathrm{B}]}$$

which gives

$$\frac{\mathrm{d[D]}}{\mathrm{d}t} = \frac{k_b k_a[\mathrm{HZ}][\mathrm{A}][\mathrm{B}]}{k_a'[\mathrm{C}] + k_b[\mathrm{B}]} \tag{A.3}$$

2nd Assumption: $k_a'[\mathrm{C}][\mathrm{MZ}] \gg k_b[\mathrm{B}][\mathrm{MZ}]$. Because water interacts stronger with the zeolite surface than benzene and the second step can only proceed when benzene drives out water, this is a logical assumption.

So finally we get

$$\frac{\mathrm{d[D]}}{\mathrm{d}t} = \frac{k_b k_a[\mathrm{HZ}][\mathrm{A}][\mathrm{B}]}{k_a' \quad [\mathrm{C}]} \tag{A.4}$$

or the global reaction rate constant, k_r, equals $k_b k_a/k_a'$. When k_b, k_a, and k_a' are expressed as the ratios of partition functions using the reaction rate theory (eq 3) we get

$$k_r = (N_A V) \times \left(\frac{k_B T}{h}\right) \cdot \frac{(Q_v^{\ddagger} Q_r Q_t)_{TS2} (Q_v Q_r Q_t)_C}{(Q_v Q_r Q_t)_A (Q_v Q_r Q_t)_B (Q_v Q_r Q_t)_{HZ}} \cdot e^{E_b + E_a - E'_a/RT} \tag{A.5}$$

which is the same as eq 5.

References and Notes

(1) Venuto, P. B. *Microporous Mater*. **1994**, *2*, 297.
(2) (a) Chen, N. Y.; Kaeding, W. W.; Dwyer, G. G. *J. Am. Chem. Soc*. **1979**, *101*, 6783. (b) Keading, W. W.; Chu, C.; Young, L. B.; Weinstein, B.; Butter, S. A. *J. Catal.* **1981**, *67*, 159.
(3) Armor, J. N. *Appl. Catal*. **1991**, *78*, 141.
(4) Song, S.; Nicholas, J. B.; Haw, J. F. *J. Am. Chem. Soc.* **2000**, *122*, 10 726.
(5) (a) Yashima, T.; Ahmad, H.; Yamazaki, K.; Katsuta, M.; Hara, N. *J. Catal*. **1970**, *16*, 273. (b) Young, L. B.; Butter, S. A.; Kaeding, W. W. *J. Catal*. **1982**, *76*, 418. (c) Derouane, E. G.; Dejaifve, P.; Gabelica, Z.; Védrine, J. C. *Faraday Discuss*. **1982**, *72*, 331. (d) Vinek, H.; Rumplmayr, G.; Lercher, J. A. *J. Catal*. **1989**, *115*, 291. (e) Vinek, H.; Lercher, J. A. *J. Mol. Catal.* **1991**, *64*, 23. (f) Espeel, P. H. J.; Vercruysse, K. A.; Debaerdemaker, M.; Jacobs, P. A. *Stud. Surf. Sci. Catal*. **1994**, *84*, 1457. (g) Fraenkel, D.; Levy, M. *J. Catal*. **1989**, *118*, 10.
(6) Denayer, J. F.; Baron, G. V.; Vanbutsele, G., Jacobs, P. A.; Martens, J. A. *J. Catal*. **2000**, *190*, 469.
(7) Haw, J. F.; Richardson, B. R.; Oshiro, I. S.; Lazo, N. L.; Speed, J. A. *J. Am. Chem. Soc.* **1989**, *111*, 2052.
(8) Tao, T.; Maciel, G. *J. Am. Chem. Soc*. **1995**, *117*, 12 889.
(9) Xu, T.; Barich, D. H.; Goguen, P. W.; Song, W.; Wang, Z.; Nicholas, J. B.; Haw, J. F. *J. Am. Chem. Soc*. **1998**, *120*, 4025.
(10) (a) Gorte, R. J. *Catal. Lett*. **1999**, *62*, 1. (b) Haw, J. F.; Xu, T.; Nicholas, J. B.; Goguen, P. W. *Nature* **1997**, *389*, 832. (c) Nicholas, J. B. *Topics Catal*. **1999**, *9*, 181.
(11) (a) Forester, T. R.; Howe, R. F. *J. Am. Chem. Soc*. **1987**, *109*, 5076. (b) Kubelkova, L.; Novakova, J.; Nedomova, K. *J. Catal*. **1990**, *124*, 441. (c) Anderson, M. W.; Klinowski, J. *J. Am. Chem. Soc*. **1990**, *112*, 10. (d) Bosacek, V.; Ernst, H.; Freude, D.; Mildner, T. *Zeolites* **1997**, *18*, 196. (e) Krossner, M.; Sauer, J. *J. Phys. Chem*. **1996**, *100*, 6199. (f) Nusterer, E.; Blöchl, P. E.; Schwarz, K. *Chem. Phys. Lett*. **1996**, *253*, 448. (g) Stich, I.; Gale, J. D.; Terakura, K.; Payne, M. C. *J. Am. Chem. Soc*. **1999**, *121*, 3292. (h) Blaszkowski, S. R.; van Santen, R. A. *J. Phys. Chem*. **1995**, *99*, 11 728. (i) Blaszkowski, S. R.; van Santen, R. A. *J. Phys. Chem. B* **1997**, *101*, 2292.
(12) Rakoczy, J.; Romotowski, T. *Zeolites*, **1993**, *13*, 256.
(13) (a) Ivanova, I. I.; Corma, A. *J. Phys. Chem. B*. **1997**, *101*, 547. (b) Mirth, G.; Lercher, J. A. *J. Phys. Chem*. **1991**, *95*, 3736. (c) Mirth, G.; Lercher, J. A. *J. Catal*. **1991**, *132*, 244.
(14) van Santen, R. A.; Kramer, G. J. *Chem. Rev*. **1995**, *95*, 637.
(15) (a) Sinclair, P. E.; Catlow, C. R. A. *J. Chem. Soc., Faraday. Trans*. **1996**, *92*, 2099. (b) Shah, R.; Gale, J. D.; Payne, M. C. *J. Phys. Chem. B*. **1997**, *101*, 4787.
(16) Beck, L. W.; Xu, T.; Nicholas, J. B.; Haw, J. F. *J. Am. Chem. Soc*. **1995**, *117*, 11 594.
(17) Heidrich, D. *Phys. Chem. Chem. Phys*. **1999**, *1*, 2209.
(18) Morrison, R. T.; Boyd, R. N. *Organic Chemistry*, Prentice Hall, New Jersey, 1992.
(19) (a) Corma, A.; Sastre, G.; Viruele, R.; Zicovich-Wilson, C. *J. Catal*. **1992**, *136*, 521. (b) Corma, A.; Sastre, G.; Viruela, P. *Stud. Surf. Sci. Catal*. **1994**, *84*, 271. (c) Corma, A.; Sastre, G.; Viruela, P. M. *J. Mol. Catal. A*. **1995**, *100*, 75.
(20) Mortier, W. J.; Ghosh, S. K.; Shankar, S. *J. Am. Chem. Soc*. **1986**, 108, 4315.
(21) Nulens, K. H. L.; Vos, A. M.; Janssens, G. O. A.; Schoonheydt, R. A. *Stud. Surf. Sci. Catal*., **2000**, 1211.
(22) Blaszkowsi, S. R.; van Santen, R. A. Alkylation and Transalkylation Reactions of Aromatics In *ACS Symposium Series 721: Transition State Modeling for Catalysis*; Thuhlar, D. G., Morokuma, K., Eds.; 1999, p 307.

(23) Vos, A. M.; Rozanska, X.; Schoonheydt, R. A.; van Santen, R. A.; Hutschka, F.; Hafner, J. *J. Am. Chem. Soc*. **2001**, *123*, 2799.

(24) (a) Becke, A. D. *J. Chem. Phys*. **1993**, *98*, 5648. (b) Lee, C.; Yang, W.; Parr, R. G. *Phys. Rev. B*, **1988**, *37*, 785.

(25) Frisch, M. J.; Trucks, G. W.; Schlegel, H. B.; Scuseria, M. A.; Robb, M. A.; Cheeseman, J. R.; Zakrzewski, V. G.; Montgomery, J. A.; Stratmann, R. E.; Burant, J. C.; Dapprich, S.; Millam, J. M.; Daniels, A. D.; Kudin, K. N.; Strain, M. C.; Farkas, O.; Tomasi, J., Barone, V., Cossi, M., Cammi, R., Mennucci, B., Pomelli, C., Adamo, C.; Clifford, S.; Ochterski, J.; Petersson, G. A.; Ayala, P. Y.; Cui, Q.; Morokuma, K.; Malick, D. K.; Rabuck, D. K.; Raghavachari, K.; Foresman, J. B.; Cioslowski, J.; Ortiz, J. V.; Stefanov, B. B.; Liu, G.; Liashenko, A.; Piskorz, P.; Komaromi, I.; Gomperts, R.; Martin, R. L.; Fox, D. J.; Keith, T.; Al-Laham, M. A.; Peng, C. Y.; Nanayakkara, A.; Gonzales, C.; Challacombe, M.; Gill, P. M. W.; Johnson, B. G.; Chen, W.; Wong, M. W.; Andress, J. L.; Head-Gordon, M.; Replogle, E. S.; Pople, J. A. *Gaussian 98 (revision A.7)* Gaussian, Inc.: Pittsburgh PA, 1998.

(26) (a) Eyring, H. *J. Chem. Phys*. **1934**, *3*, 107. (b) Glasstone, S. *Physical Chemistry*; D. Van Nostrand Company, Inc: Toronto, 1946. (c) Robinson, P. J. *J. Chem. Educ*. **1978**, *55*, 509.

(27) Scott, A. P.; Radom, L. *J. Phys. Chem*. **1996**, *100*, 16 502.

(28) (a) Parr, R. G.; Yang, W. *Density Functional Theory of Atoms and Molecules*; Oxford University Press: Oxford, 1989. (b) Parr, R. G.; Yang, W. *Annu. Rev. Phys. Chem*. **1995**, *46*, 701.

(29) Pearson, R. G.; Parr, R. G. *J. Am. Chem. Soc*. **1983**, *105*, 7512.

(30) Parr, R. G.; Yang, W. *J. Am. Chem. Soc*. **1984**, *106*, 4049.

(31) Fukui, K.; Yonezawa, T.; Shingu, H. *J. Chem. Phys*. **1952**, *20*, 722.

(32) Yang, W.; Mortier, W. J. *J. Am. Chem. Soc*. **1986**, *108*, 5708.

(33) Breneman, C. M.; Wiberg, K. B. *J. Comput. Chem*. **1990**, *11*, 361.

(34) Yang, W.; Parr, R. G. *Proc. Nat. Acad. Sci. U. S.A*. **1985**, *82*, 6723.

(35) (a) Gazquez, J. L.; Mendez, F. *J. Phys. Chem*. **1994**, *98*, 4591. (b) Damoun, S.; Van de Woude, G.; Mendez, S.; Geerlings, P. *J. Phys. Chem. A* **1997**, *101*, 886. (c) Geerlings, P.; De Proft, F. *Int. J. Quantum Chem*. **2000**, *80*, 227.

(36) Pearson, R. G. *Hard and Soft Acids and Bases*, Dowen, Hutchinson and Ross, Stroudsberg, 1973.

(37) Berkowitz, M.; Ghosh, S. K.; Parr, R. G. *J. Am. Chem. Soc*. **1985**, *107*, 6811.

(38) Harbola, M. K.; Chattaraj, P. K.; Parr, R. G. *Isr. J. Chem*. **1991**, *31*, 395.

(39) (a) Langenaeker, W.; De Proft, F.; Geerlings, P. *J. Phys. Chem*. **1995**, *99*, 6424. (b) Geerlings, P.; Langenaeker, W.; De Proft, F.; Baeten, A. *Molecular Electrostatic Potentials vs DFT descriptors of reactivity* in Molecular Electrostatic Potentials − Concepts and Applications (Theoretical and Computational Chemistry, Vol. 3), 1996, 587.

(40) Vos, A. M.; De Proft, F.; Schoonheydt, R. A.; Geerlings, P. *Chem. Commun*. **2001**, *11*, 1108.

(41) Kramer, G. J.; van Santen, R. A.; Emeïs, C. A.; Nowak, A. K. *Nature* **1993**, *363*, 529.

(42) Schoofs, B.; Martens, J. A.; Jacobs, P. A.; Schoonheydt, R. A. *J. Catal*. **1999**, *183*, 355.

(43) Pearson, R. G. *J. Chem. Educ*. **1987**, *64*, 561.

(44) Zhou, Z.; Parr, R. G. *J. Am. Chem. Soc*. **1990**, *112*, 5720.

(45) (a) Michalak, A.; De Proft, F.; Geerlings, P.; Nalewajski, R. *J. Phys. Chem. A* **1999**, *103*, 762. (b) Balawender, R.; De Proft, F.; Komorowski, L.; Geerlings, P. *J. Phys. Chem. A* **1998**, *102*, 9912.

(46) (a) Le, T. N.; Nguyen, L. T.; Chandra, A. K.; De Proft, F.; Geerlings, P.; Nguyen, M. T. *J. Chem. Soc., Perkin Trans*. **1999**, *2*, 1249. (b) Nguyen, L. T.; Le, T. N.; De Proft, F.; Chandra, A. K.; Langenaeker, W.; Nguyen, M. T.; Geerlings, P. *J. Am. Chem. Soc*. **1999**, *121*, 5992.

(47) Atkins, P. W. *Physical Chemistry*; Oxford University Press: New York, 1998, p 784−786.